COMPONENTS FOR BATCH-FABRICATED CHIP-SCALE ATOMIC CLOCKS

M. H. Kwakernaak, S. Lipp, S. McBride, P. Zanzucchi, W.K. Chan, V.B. Khalfin, H. An, R. D. Whaley, Jr., B. I. Willner, A. Ulmer, J. Z. Li, T. Davis, A. M. Braun, J. H. Abeles
Sarnoff Corporation, 201 Washington Road, Princeton NJ 08543, USA
E-mail: ***mkwakernaak@sarnoff.com***

A. Post, Y-Y. Jau, N. N. Kuzma, and W. Happer
Department of Physics, Princeton University, Princeton NJ 08544, USA

Abstract

We describe chip-scale batch-fabricated cesium cells utilizing semiconductor wafer processing, pin transfer of cesium, and silicon/Pyrex anodic bonding for cell sealing. High-speed, single-mode linearly polarized VCSELs emitting at the ^{133}Cs D1 line were fabricated, optimized for low threshold and high-speed operation with overall small power dissipation. Coherent population trapping (CPT) end-resonance signals with a contrast and linewidth of 5.4% and 7.1 kHz respectively are achieved using 1 mm optical path length cells and VCSEL driven with 1.25 mW RF modulation and 2.76 mW DC power dissipation. We demonstrate short-term stability of $4.5\times10^{-10}\cdot\tau^{-1/2}$ with an atomic clock built with these components operating on the CPT end-resonance. The magnetic field is stabilized with a novel magnetic field locking scheme tapping the Zeeman resonance.

INTRODUCTION

Atomic time and RF frequency references are important for applications such as jam-resistant global positioning and communication networks. Increasingly, stable frequency references with small size and low power consumption are desirable. The most promising approach to realize atomic clocks with cm dimensions and mW-range power dissipation is coherent population trapping (CPT), eliminating the need for a microwave cavity and therefore enabling a compact physics package **[1]**. With CPT, coherent optical tones with frequency difference equal to the hyperfine frequency are utilized to resonantly pump the alkali vapor. For reduced power dissipation, small cell sizes with reduced surface area decrease radiative losses, and low power; high-efficiency lasers reduce conductive losses. We have developed batch-fabricated cesium micro-cells and low-power Vertical Cavity Surface Emitting Lasers (VCSELs) that are key components for enabling dramatic reduction in size and power of such clocks.

Atomic vapor cells are traditionally made using glass-blowing techniques. Besides the relatively large size of such cells, individual fabrication makes them unsuitable for economic production in large quantities. Taking advantage of semiconductor wafer processing techniques, we developed batch

fabrication of miniaturized alkali vapor cells. Anodic bonding has been used for sealing micro-machined miniature cells **[2]**. We use this technique for wafer-scale cell array sealing.

Compact low-power cesium atomic clocks based on coherent population trapping (CPT) require modulated laser sources at 852 or 894 nm for optical pumping of alkali-vapor cells, using the D2 or D1 atomic transitions, respectively **[3]**. In the past, 852 nm VCSELs available as a by-product of data communication applications have been used experimentally to pump the ^{133}Cs D2 optical transition **[4]**. However, the D1 transition at 894 nm yields ~10 times the signal strength **[3]** for improved clock demonstrations **[5,6]**. For ultra-compact clocks, low power dissipation is required at optical output power levels of 1 μW - 100 μW. We fabricated VCSELS operating on the ^{133}Cs D1 line that, when biased at ~1.5 mA, exhibit the ability to be modulated at either the ^{133}Cs hyperfine transition frequency (near 9.2 GHz) or its first sub-harmonic (near 4.6 GHz).

Modulation optical pumping schemes using coherent population trapping (CPT) have been demonstrated using VCSELs and miniature cells **[1,6]**. Typically the magnetic field independent hyperfine transition, $m_F = 0 \rightarrow 0$, is used. However, due to optical pumping with circularly polarized light, spin population tends to depopulate out of the 0-0 transition and aggregate in the end-transition. Further, due to conservation of angular momentum, this end-transition state suppresses spin-exchange hyperfine linewidth broadening, a dominant linewidth broadening mechanism in small, high-temperature 0-0-based clocks. Therefore, significantly improved contrast and linewidth of the CPT resonance signal, both of which influence the short-term clock stability, can be achieved by using the end-resonance **[7-9]**. A magnetic field feedback loop, which utilizes the Zeeman resonance, stabilizes the end-transition against magnetic field perturbations.

WAFER-SCALE CESIUM MICROCELL FABRICATION

Wafer-scale cesium microcells were batch-fabricated utilizing semiconductor wafer processing, cesium pin transfer, and Pyrex/silicon anodic bonding. The fabrication process is outlined in Figure 1. A Si_3N_4 etch mask is lithographically patterned and defined with RIE on both sides of a 1 mm thick double side polished silicon wafer. Holes are wet chemically etched through the silicon wafer with KOH:1-Propanol:H_20. Pyrex is anodically bonded at a temperature of 425ºC to the patterned silicon wafer using a voltage of 1 kV (step 1 in Figure 1). The wafer is transferred into a glove box containing buffer-gas atmosphere at a temperature of 35ºC. We used N_2 buffer gas for the present cells. The cells receive droplets of liquid cesium by pin transfer (step 2 in Figure 1). Finally, a second Pyrex plate is anodically bonded at 300ºC to seal the cells. A photograph of the completed cesium cells is shown in Figure 2. The cell outer aperture is 3 × 3 mm with a path length of 1 mm.

HIGH-SPEED 894 NM VCSEL FOR CS D1 TRANSITIONS

The VCSELs are grown with MOCVD on 2-degree off-axis GaAs substrates. The fabricated VCSELs (Figure 3) include three InGaAs quantum wells and two oxide apertures, one above and one below the active region. The wet oxidation layer is $Al_{0.95}Ga_{0.05}As$. The 21 top mirror layers and 31 bottom mirror layer pairs ($Al_{0.9}Ga_{0.1}As$ and $Al_{0.06}Ga_{0.94}As$) are undoped to obtain low absorption loss and low threshold as well as high relaxation oscillation frequencies at low bias currents. Current is injected through ohmic contacts on two intra-cavity contact layers ($Al_{0.06}Ga_{0.94}As$), which are placed above and below the oxide apertures. For high-speed modulation, coplanar strip lines are patterned on the GaAs wafer surface.

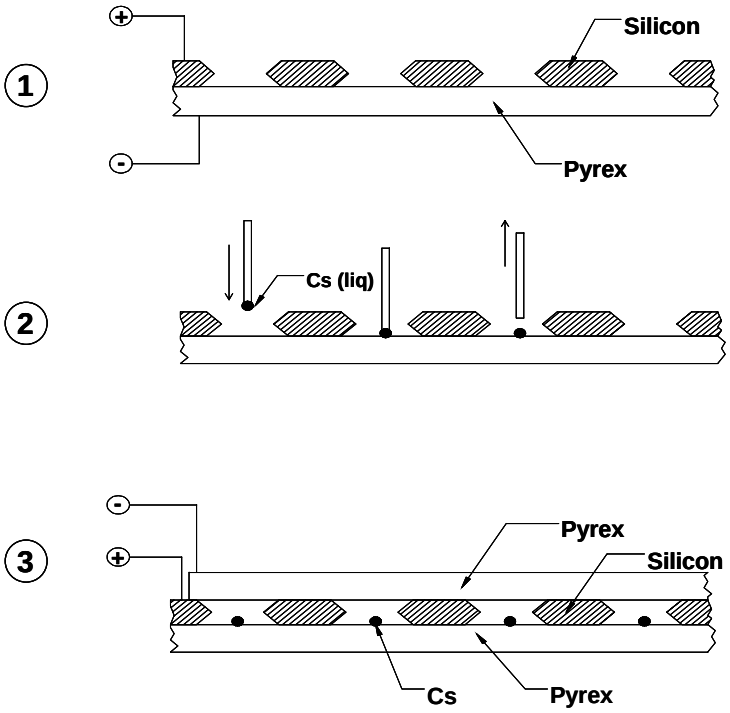

Figure 1. Schematic description of ^{133}Cs cell fabrication. Step 1: Silicon wafer patterning and thru-etching subsequent to anodic bonding with Pyrex plate. Step 2: Within buffer gas environment, metallic cesium droplet is placed in wells via a pin transfer technique. Step 3: Batch cell sealing with anodic bonding of top Pyrex plate to silicon.

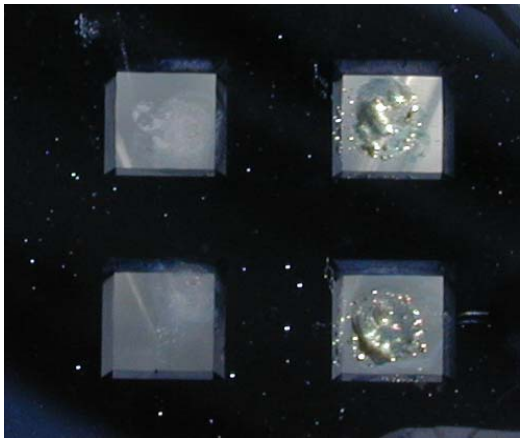

Figure 2. Close-up image of an array of completed cesium cells. Cesium metal can be seen within the cells. In this array, 380 torr (20°C) N_2 buffer gas was used.

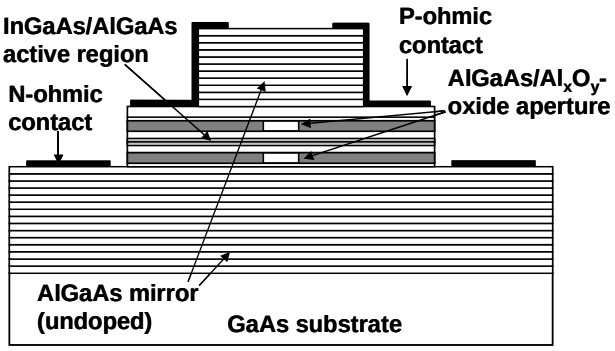

Figure 3. Schematic of the intra-cavity contact dual oxide aperture VCSELs.

The oxide aperture diameter is 4 μm. Measured power versus current relation is shown in Figure 4. At room temperature the threshold current is 550 μA and the slope-efficiency is 0.17 W/A. The differential series resistance is 280 Ω. The modulation response (Figure 5a) shows that a 10 GHz bandwidth is obtained with only 1.5 mA injection current. For efficient 4.6 GHz modulation, a bias current of 0.8 mA is sufficient. The side-mode suppression exceeds 20 dB at currents up to 2.6 mA (350 μW output power). High-resolution optical spectra (Figure 5b) show that at 1 dBm modulation power (9.2 GHz) the total side band power equals the carrier power. Total power consumption in this case is 3.3 mW DC and 1.25 mW RF.

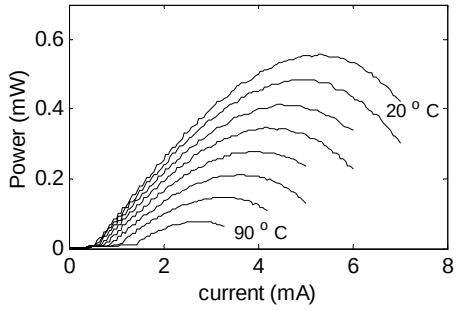

Figure 4. Power versus current measured for temperatures from 20ºC to 90ºC in steps of 10ºC.

END-RESONANCE ATOMIC CLOCK

Typically, the two field independent sublevels of the atomic vapor with angular momentum quantum number m_F=0 are used (Figure 6). Strong optical pumping with circularly polarized light at the D1 wavelength transfers most atoms into the end states (F=4, m_F=-4 and F=3,m_F=-3 in Figure 6). As a result, the CPT signal strength increases. In addition, as the end-transition is a maximum angular momentum state, collisions between atoms in the end states do not result in a change of spin population concentration and, hence, minimize the overall spin exchange collisional broadening **[9]**. This is particularly relevant in

miniature cells operating at elevated temperatures and high alkali-vapor densities.

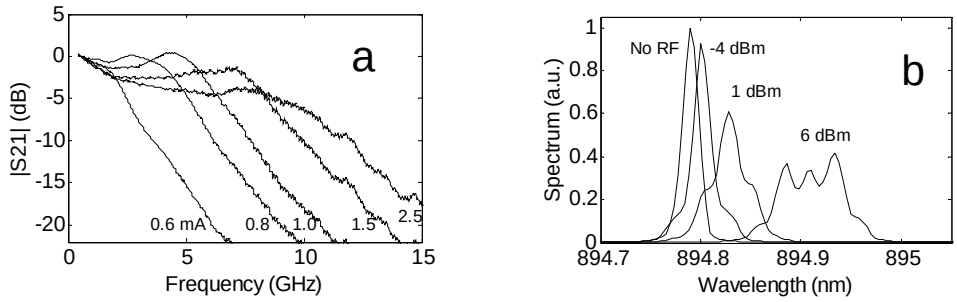

Figure 5. a) Frequency response for bias currents of 0.6 mA, 0.8 mA, 1 mA, 1.5 mA, and 2.5 mA. b) Optical spectrum measured with 0.01 nm resolution without modulation and with -4 dBm, 1 dBm, and 6 dBm modulation at 9.2 GHz.

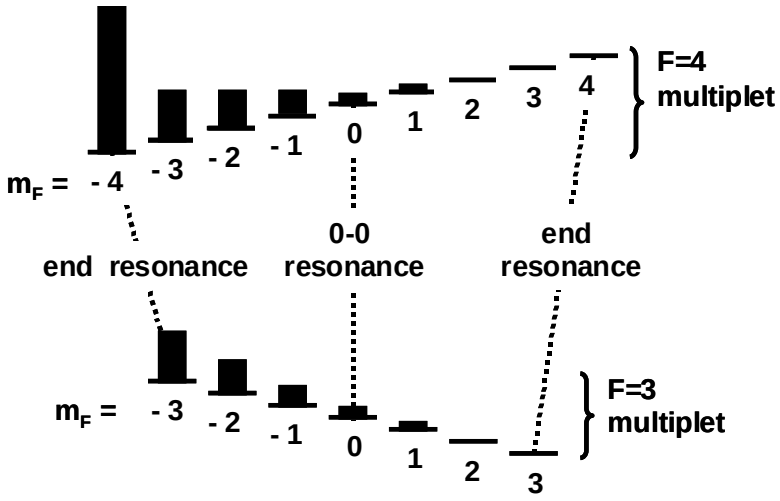

Figure 6. Schematic of ground state hyperfine levels of ^{133}Cs and populations at strong circularly polarized optical pumping.

Although the CPT signal can be improved (increased signal strength, reduced linewidth as compared to 0-0), a drawback of this scheme is the first-order dependence of the end-resonance frequency on the magnetic field. While the second-order frequency shift in 0-0 clocks is sufficiently small to be suppressed with adequate magnetic field shielding, end-resonance clocks require active control of the magnetic field. To stabilize the magnetic field, the Zeeman resonance of the cesium can be used (F=4, m_F=-4 → m_F=-3 in Figure 6). The Zeeman frequency shift is proportional to the magnetic field. Therefore, locking the Zeeman frequency to a stable oscillator locks the field.

A schematic of the clock configuration is shown in Figure 7. A high-speed VCSEL at the ^{133}Cs D1 absorption line pumps the miniature cell. The transmission is detected with a silicon photodiode. The

VCSEL and the cell are both temperature-controlled. The schematic shows three feedback loops. One locks the VCSEL wavelength to the D1 absorption, the second locks a local oscillator to the CPT end-resonance frequency, and the third controls the magnetic field. All three loops use synchronous detection of different frequencies.

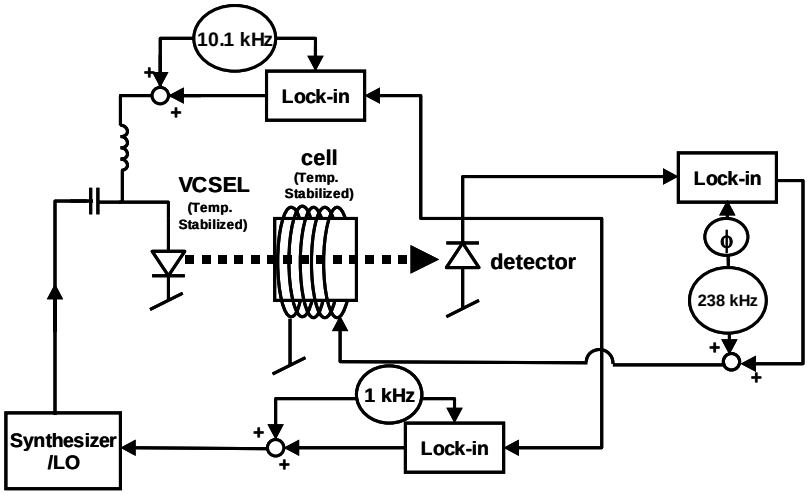

Figure 7. Schematic of atomic clock configuration. Three feedback loops utilize synchronous detection at different frequencies. A feedback loop locks the VCSEL wavelength to the ^{133}Cs D1 absorption (at 10.1 kHz), a feedback loop stabilizes the magnetic field (at 238 kHz), and the local oscillator to provide the clock frequency is locked into the CPT end-resonance (at 1 kHz).

END-RESONANCE CPT WITH MICRO-CELL AND VCSEL

The miniature Cs cell has a window of 3 × 3 mm and an optical path length of 1 mm. The cell is filled with N_2 buffer gas with a pressure of 380 torr (at 20°C) and is temperature-stabilized at 100 °C. In the experiments described below, the VCSEL is driven with a bias current of 1.2 mA. The DC VCSEL power is 2.76 mW. The optical power in the cell is 100 μW. The VCSEL is modulated with 1.25 mW RF power at 4.5957 GHz. This is one half of the hyperfine end-resonance. A constant magnetic field of 0.7 G is applied at an angle of 45° with respect to the light direction.

Figure 8 shows the measured optical transmission spectrum of the cell. This measurement was performed with all three feedback loops open. The optical frequency of the VCSEL changes with current at a rate of 300 GHz/mA. For this measurement, the VCSEL current was tuned to scan the wavelength over the cesium absorption while the photocurrent was measured. Although broadened by ~8 GHz, the hyperfine structure is still visible. 1 dBm RF modulation of the VCSEL current transfers a significant portion of the light into the modulation sidebands. This is most visible in the difference of the transmission measurements with RF modulation off and on (Figure 8, dashed and solid line).

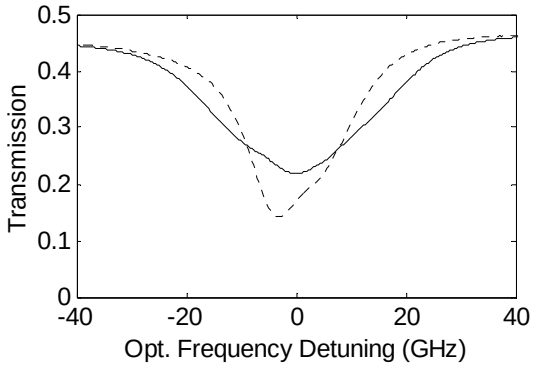

Figure 8. Optical transmission spectrum through the cell obtained by current tuning the VCSEL wavelength across the ^{133}Cs absorption. Dashed: No modulation applied to the VCSEL. Solid: The VCSEL is modulated with 1 dBm RF Power at 4.5957 GHz, slightly detuned from the CPT resonance.

The VCSEL wavelength is locked into the absorption peak by applying a small current modulation to the VCSEL that results in a wavelength modulation, and using synchronous detection as shown in Figure 7. Photodiode current noise measured at 1 kHz with the VCSEL locked to the cesium absorption is shown in Figure 9. Increase in noise detuned from the absorption indicates FM noise of the VCSEL light converted into intensity noise on the absorption spectrum slope **[10]**. However, in our measurements, due to the substantially broadened Cs lines, the noise is dominated by relative intensity noise of the VCSEL itself at the absorption peak. Shot noise, which is normalized to the photocurrent at 0.17×10^{-6} Hz$^{-1/2}$, and thermal noise of the detector and subsequent amplifier are insignificant because of the comparably high optical power used in this end-resonance scheme. The VCSEL relative intensity noise of –104 dBc$^{-1/2}$ Hz at 1 kHz drops on a ~1/f slope to -130 dBc$^{-1/2}$ Hz at 200 kHz, a range of VCSEL noise reported elsewhere **[11]**.

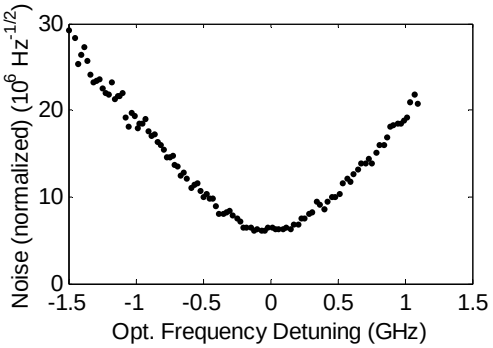

Figure 9. Photocurrent noise at 1 kHz normalized to the DC photocurrent. The VCSEL wavelength is locked to the absorption and tuned by adding an offset to the feedback.

Figure 10 shows the measured end-resonance CPT signal obtained with 1 dBm RF modulation of the VCSEL. The resulting contrast and linewidth are 5.4% and 7.1 kHz respectively. Also shown is the CPT

error signal. This error is obtained by adding an FM dither modulation with 6 kHz peak-to-peak excursion at 1 kHz to the RF modulation and synchronous detection at the dither frequency.

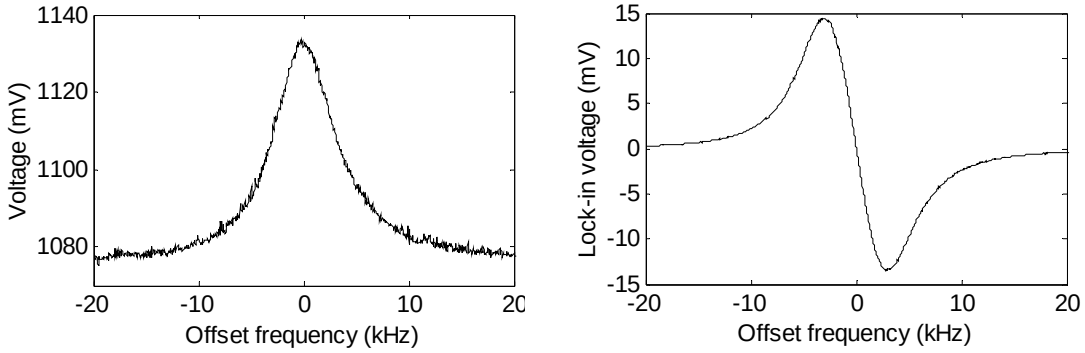

Figure 10. Left: Measured end-transition CPT resonance signal utilizing high speed VCSEL, and 1 mm thick cesium cell. Contrast and linewidth are 5.4% and 7.1 kHz respectively. Offset frequencies are relative to 4.5957 GHz. Right: Error signal obtained by adding a 1 kHz FM dither to the RF modulation and synchronous detection in a lock-in amplifier.

MAGNETIC FIELD CONTROL

While compensating for external field fluctuations, the addition of a control loop to stabilize the magnetic field may actually add noise to the magnetic field and, thus, the end-resonance frequency. This could result in an impairment of the short-term clock stability. The noise spectral density of the clock frequency is **[12]**:

$$S_f = \frac{S_{Nf}}{\left|\frac{de_f}{df_{lo}}\right|^2} + S_{fe}$$

where S_f is the clock frequency noise spectral density, S_{Nf} is the noise spectral density of the frequency loop error signal, e_f is the frequency loop error signal, and f_{lo} is the local oscillator frequency. de_f / df_{lo} is the slope of the error signal at the lock point. S_{fe} is the noise spectral density of the end-resonance frequency. The shift of the end-resonance frequency with magnetic field translates magnetic field noise into noise of the end-resonance frequency.

Provided that a stable oscillator is available to sense the Zeeman frequency, feedback will stabilize the magnetic field against external fluctuations, but will leave a residual magnetic field noise spectral density S_B of:

$$S_B = \frac{S_{NB}}{\left|\frac{de_B}{dB}\right|^2}$$

where e_B is the error signal of magnetic field feedback system, B is the magnetic field, and de_B/df_B is the slope of the magnetic field error signal at the lock point. S_{NB} is the noise spectral density in the detection of the error signal. In our scheme, the Zeeman resonance of the atomic vapor is used to measure the magnetic field, and the CPT end-resonance frequency is detected by modulating the VCSEL at one half the end-resonance frequency. If f_e is interpreted as this half end-resonance frequency, f_e and f_z shift with the magnetic field as:

$$\frac{df_e}{dB} = \frac{7}{2} \cdot \frac{df_z}{dB}$$

Using this and the identities above, the noise spectrum of the clock output frequency, including contributions from magnetic field noise, is:

$$S_f = \frac{S_{Nf}}{\left|\frac{de_f}{df}\right|^2} + \frac{7}{2}\frac{S_{NB}}{\left|\frac{de_B}{df_{zlo}}\right|^2}$$

Both S_{Nf} and S_{NB} can be considered white noise in the frequency range of interest, since both signals are obtained through synchronous detection in a narrow band. The Allan variance of the clock frequency is then:

$$\sigma^2(\tau) = \frac{1}{2 f_e^{\,2} \tau}\left(\frac{S_{Nf}}{\left|\frac{de_f}{df}\right|^2} + \frac{7}{2}\frac{S_{NB}}{\left|\frac{de_B}{df_z}\right|^2}\right)$$

In the atomic clock, a stable frequency reference is available with the clock output frequency. It can be easily shown that if the frequency used to measure the Zeeman resonance is synthesized from the clock output frequency, the contribution of this oscillator noise is irrelevant.

A configuration to measure the Zeeman resonance is shown in Figure 11. An oscillator modulates the current in a coil around the cesium cell at the Zeeman frequency, resulting a magnetic field modulation of ~1 mG. As a result, the light picks up the modulation in the cell **[13]**. This modulation is synchronously detected with a lock-in amplifier.

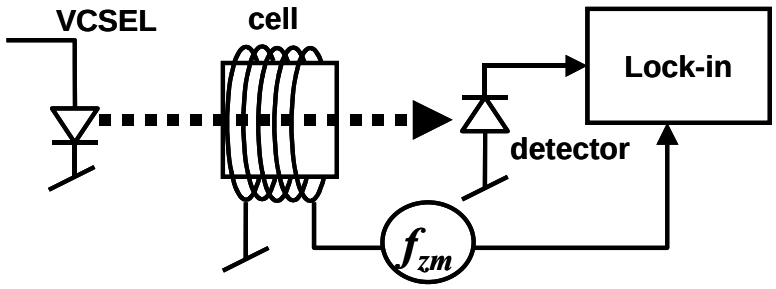

Figure 11. Configuration for the measurement of the Zeeman resonance.

Measured lock-in signal versus excitation frequency is shown in Figure 12. With proper adjustment of the lock-in phase, an anti-symmetric signal around the Zeeman frequency (at 238 kHz) is obtained (solid line in Figure 12). Keeping the oscillator frequency fixed and scanning the magnetic field results in a similar characteristic, since the Zeeman frequency and the B-field have a linear relation (350.3 kHz/G for cesium). The anti-symmetry around the Zeeman resonance allows direct use of this signal as a correction signal to a coil to adjust the magnetic field. Since there is no additional dithering required, detection is at 238 kHz despite the 5 kHz Zeeman linewidth. As a result of this and the 1/f drop of the VCSEL relative intensity noise, the signal-to-noise ratio of the magnetic field feedback improves substantially compared to a dithering approach.

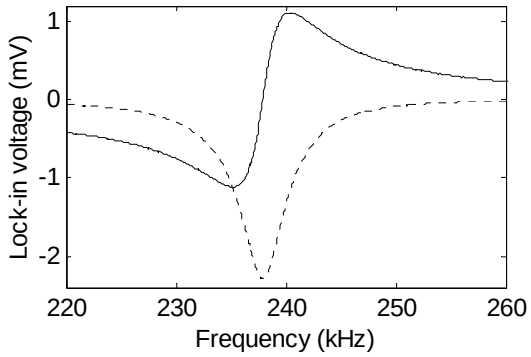

Figure 1. Zeeman signal synchronously detected with a lock-in amplifier versus magnetic field modulation frequency. Solid and dashed lines are the two lock-in components with 90° phase difference with respect to each other.

CLOCK RESULTS

In the complete clock, the three described feedback loops operate on sufficiently separated frequencies to avoid mutual interference: the CPT frequency loop at 1 kHz, the VCSEL wavelength lock at 10.1 kHz, and the Zeeman magnetic-field stabilization loop at 238 kHz. The Allan deviation of the complete clock is shown in Figure 13. Also shown is the short-term stability calculated from open loop measured signal-to- noise ratios of both the frequency loop and the B-field stabilization loops. Short-term stability is on a $4.5 \cdot 10^{-10} \cdot \tau^{-1/2}$ slope, satisfying our design goal, which is $6 \cdot 10^{-10} \cdot \tau^{-1/2}$. We attribute the drift component in the measurement to the N_2 buffer gas, which is not temperature-compensated, and imperfect temperature control of the cell.

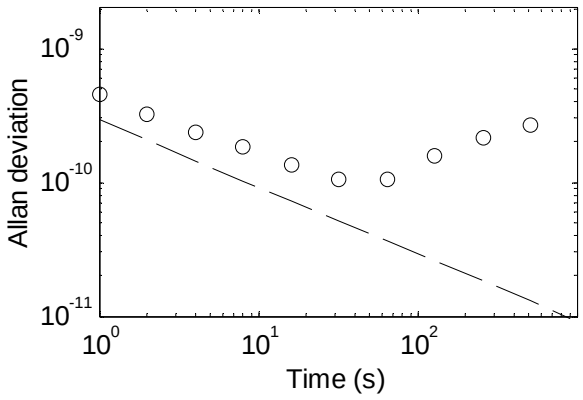

Figure 13. Allan deviation of end-resonance CPT clock with magnetic field locking. Circles are measured data; the dashed line is calculated from signal-to-noise measured in open-loop configuration.

CONCLUSIONS

Semiconductor wafer processing enables batch fabrication of cesium micro-cells for atomic clocks. Pin transfer of cesium and Pyrex-silicon anodic bonding was demonstrated to be a powerful way to fill and seal wafer scale cesium cell arrays. We demonstrated high-speed, single-mode ^{133}Cs D1 line VCSELs, which operate with just 2.76 mW DC power dissipation and 1.25 mW RF modulation at 4.6 GHz to provide adequate signal levels with the cesium micro-cells. We achieved end-resonance CPT signals with the VCSEL and a 1 mm path length cell with a contrast and linewidth of 5.4% and 7.1 kHz respectively. We demonstrated magnetic field locking by means of locking the Zeeman resonance of the cesium vapor. This mitigates the magnetic field dependence of the end-resonance frequency and allows taking advantage of enhanced end-resonance signals in a clock. We demonstrated short-term stability of $4.5 \cdot 10^{-10} \cdot \tau^{-1/2}$ with an atomic clock built with these components operating on the CPT end-resonance and utilizing the magnetic field control.

ACKNOWLEDGMENTS

The research reported in this document was performed by Sarnoff Corporation in connection with contract/instrument NBCHC020045 with the Department of the Interior.

REFERENCES

[1] S. Knappe, V. Shah, P. D. D. Schwindt, L. Hollberg, J. Kitching, L. A. Liew, and J. Moreland, 2004, *"A Microfabricated Atomic Clock,"* **Applied Physics Letters, 85,** 1460-1462.

[2] L-A. Liew, S. Knappe, J. Moreland, H. Robinson, L. Hollberg, and J. Kitching, 2004, *"Microfabricated Alkali Atom Vapor Cells,"* **Applied Physics Letters, 84,** 2694-2696.

[3] W. Happer, 1972, *"Optical Pumping,"* **Reviews of Modern Physics, 44,** 169-249.

[4] J. Kitching, L. Hollberg, S. Knappe, and R. Wynands, 2001, *"Compact Atomic Clock Based on Coherent Population Trapping,"* **Electronics Letters, 37,** 1449-1451.

[5] M. Stahler, R. Wynands, S. Knappe, J. Kitching, L. Hollberg, A. Taichenachev, and V. Yudin, 2002, *"Coherent Population Trapping Resonances in Thermal 85Rb Vapor: D1 vs. D2 Line Excitation,"* **Optics Letters, 27,** 1472-1474.

[6] R. Lutwak, D. Emmons, T. English, W. Riley, A. Duwel, M. Varghese, Charles Stark, D. K. Serkland, and G. M. Peake, 2003, *"The Chip-Scale Atomic Clock - Recent Development Progress,"* in Proceedings of the 34th Annual Precise Time and Time Interval (PTTI) Systems and Applications Meeting, 3-5 December 2002, Reston, Virginia, USA (U.S. Naval Observatory, Washington, D.C.), pp. 539-550.

[7] Y.-Y. Jau, A. B. Post, N. N. Kuzma, A. M. Braun, M. V. Romalis, and W. Happer, 2003, *"The Physics of Miniature Atomic Clocks: 0-0 Versus End Resonances,"* in Proceedings of the 2003 IEEE International Frequency Control Symposium and PDA Exhibition Jointly with the 17th European Frequency and Time Forum (EFTF), 5-8 May 2003, Tampa, Florida, USA (IEEE 03CH37409C), pp. 33-36.

[8] A. B. Post, Y-Y. Jau, N. N. Kuzma, A. M. Braun, S. Lipp, J. H. Abeles, M. V. Romalis, E. Miron, and W. Happer, 2003, "End Resonance for Atomic Clocks," in Proceedings of the 34th Annual Precise Time and Time Interval (PTTI) Systems and Applications Meeting, 3-5 December 2002, Reston, Virginia, USA (U.S. Naval Observatory, Washington, D.C.), pp. 445-456.

[9] Y.-Y. Jau, A. B. Post, N. N. Kuzma, A. M. Braun, M. V. Romalis, and W. Happer, 2004, *"Intense, Narrow Atomic-Clock Resonances,"* **Physical Review Letters, 92** (11): 110801.

[10] J. Kitching, S. Knappe, N. Vukicevic, L. Hollbreg, R. Wynands, and W. Weidmann, 2000, *"A Microwave Frequency Reference Based on VCSEL-Driven Dark Line Resonance in Cs Vapor,"* **IEEE Transactions on Instrumentation and Measurement, IM-49,** 1313-1317.

[11] C. Carlsson, H. Martinsson, R. Schatz, J. Halonen, and A. Larsson, 2002, *"Analog Modulation Properties of Oxide Confined VCSELs at Microwave Frequencies,"* **IEEE Journal of Lightwave Technology, 20,** 1740-1749.

[12] J. Vanier and C. Audoin, 1989, **The Quantum Physics of Frequency Standards** (Adam Hilger, Bristol and Philadelphia).

[13] W. E. Bell, and A. L. Bloom, 1957, *"Optical Detection of Magnetic Resonance in Alkali Metal Vapor,"* **Physical Review, 107** (6), 1559-1565.

QUESTIONS AND ANSWERS

JOHN VIG (U.S. Army CERDEC): When does your Phase II end? And it is not clear from your presentation as to how you are doing with respect to meeting the Phase II goals. The Phase II goals are pretty demanding, right?

MARTIN KWAKERNAAK: Right.

VIG: And, it seems to me, you only have a few months left to meet those goals.

KWAKERNAAK: In this presentation, we just talk about the VCSEL and the cell and how a clock performs in our lab setup. There is a lot more work to do to assemble these devices into a complete package to form a miniaturized clock, that's right.

JIM CAMPARO (The Aerospace Corporation): You showed that you are doing the end-to-end pumping to improve the signal amplitude. Have you been able to do any estimates of the magnitude improvement you get by going to the end-to-end pumping, as opposed to not using circulating polarized light to zero-zero. How much do the signals improve by that?

KWAKERNAAK: This question is not so simple because the optimum performance is different. It depends on the cell conditions, what kind of preference. It is different for end resonance and zero-zero. But we think we get an improvement of factor five or ten at least.

SVENJA KNAPPE (National Institute of Standards and Technology): I would be interested to know if you have any data on how reliable the VCSELs are you developed in terms of lifetime.

KWAKERNAAK: No, we did not do any lifetime studies on these VCSELs.